

# **FINAL REPORT STTR PHASE I**

## ***An Automated Design Optimization Tool for Electromagnetic Control of Hypersonic Flows***

**Contract No. FA9550-04-C-0105**

Contractor: ZONA Technology, Inc.  
7430 E. Stetson Drive, Suite 205  
Scottsdale, AZ 85251-3540  
Tel (480) 945-9988 / Fax (480) 945-6588

Issued by: USAF/AFMC  
Air Force Office of Scientific Research  
801 North Randolph Street, Room 732  
Arlington, VA 22203-1977

Program Manager: John Schmisser  
Air Force Office of Scientific Research  
801 North Randolph Street, Room 732  
Arlington, VA 22203-1977

Contract No. FA9550-04-C-0105  
STTR Topic No.: AF04-T009  
Report No.: 0003  
Item No. 0003AA  
Start Date: September 1, 2004  
End Date: May 31, 2005



**20050804 005**

## REPORT DOCUMENTATION PAGE

0313

The public reporting burden for this collection of information is estimated to average 1 hour per response, including the gathering and maintaining the data needed, and completing and reviewing the collection of information. Send comments regarding this burden estimate or any other aspect of this collection of information, including suggestions for reducing the burden, to Department of Defense, Washington Headquarters Services, Directorate for Information Operations and Reports (0704-0188), 1215 Jefferson Davis Highway, Suite 1204, Arlington, VA 22202-4302. Respondents should be aware that notwithstanding any other provision of law, no person shall be subject to any penalty for failing to comply with a collection of information if it does not display a currently valid OMB control number.

PLEASE DO NOT RETURN YOUR FORM TO THE ABOVE ADDRESS.

1. REPORT DATE (DD-MM-YYYY) 15-06-2005			2. REPORT TYPE FINAL		3. DATES COVERED (From - To) Sept 1, 2004 - May 31, 2005	
4. TITLE AND SUBTITLE An Automated Design Optimization Tool for Electromagnetic Control of Hypersonic Flows					5a. CONTRACT NUMBER FA9550-04-C-0105	
					5b. GRANT NUMBER	
					5c. PROGRAM ELEMENT NUMBER	
6. AUTHOR(S) Drs. Lei Tang, Yun Zheng, and Danny D. Liu ZONA Technology, Inc. Dr. Juan J. Alonso and Mr. Andre C. Marta Stanford University Dr. K. Xu Hong Kong University of Science and Technology					5d. PROJECT NUMBER	
					5e. TASK NUMBER	
					5f. WORK UNIT NUMBER	
7. PERFORMING ORGANIZATION NAME(S) AND ADDRESS(ES) ZONA Technology, Inc. 7430 E. Stetson Drive, Ste. 205 Scottsdale, AZ 85251-3540 Tel 480-945-9988 / Fax 480-945-6588 / URL: www.zonatech.com					8. PERFORMING ORGANIZATION REPORT NUMBER Z05-08	
9. SPONSORING/MONITORING AGENCY NAME(S) AND ADDRESS(ES) Air Force Office of Scientific Research ATTN: John Schmisser -NA 875 North Randolph Street Suite 325, Room 3112 Arlington, Virginia 22203					10. SPONSOR/MONITOR'S ACRONYM(S)	
					11. SPONSOR/MONITOR'S REPORT NUMBER(S)	
12. DISTRIBUTION/AVAILABILITY STATEMENT Approved for public release, distribution unlimited						
13. SUPPLEMENTARY NOTES						
14. ABSTRACT There has been computational work to analyze and control hypersonic flows using electromagnetic effects but no true effort has been pursued to automate the flow control process. The lack of a design framework that provides automated multi-disciplinary optimization (MDO) capabilities for this class of problems is the principal motivation for this work. This project develops the foundation of one of the principal components of such MDO environment.  Control theory, which has already proved successful dealing with both aerodynamic shape and aero-structural optimization problems, is extended to magnetohydrodynamics (MHD). The discrete adjoint approach emerges as the best suitable option to deal with the complex equations that govern MHD, and with the nature of the cost functions that may be used for relevant design problems.  The equations governing the three-dimensional flow of a compressible conducting fluid in a magnetic field using the low magnetic Reynolds number approximation are solved with a gas-kinetic BGK scheme. Compared with the more conventional continuum CFD approach, a gas-kinetic CFD approach can be easily extended beyond the continuum regime.						
15. SUBJECT TERMS Hypersonic, Magnetohydrodynamics, Design optimization, Gas-kinetic schemes, Adjoint optimization methods						
16. SECURITY CLASSIFICATION OF:			17. LIMITATION OF ABSTRACT SAM	18. NUMBER OF PAGES	19a. NAME OF RESPONSIBLE PERSON Dr. Lei Tang	
a. REPORT U	b. ABSTRACT U	c. THIS PAGE U			19b. TELEPHONE NUMBER (Include area code) 480-945-9988	

7/29/05

***An Automated Design Optimization Tool  
for Electromagnetic Control of Hypersonic Flows***

**Contract No. FA9550-04-C-0105**

**Final Report Period (09/01/04 ~ 05/31/05)**

**Table of Contents**

- 1.0 Activity Summary**
- 2.0 BGK-NS Scheme for Magnetogasdynamics in Thermal and Chemical Equilibrium**
- 3.0 Adjoint Optimization Method for Magnetogasdynamics in Thermal and Chemical Equilibrium**
- 4.0 BGK-Burnett Scheme for Gas Dynamics in Thermal and Chemical Equilibrium**
- 5.0 Generalization of Gas-Kinetic Navier-Stokes Solver to Hypersonic Flows in Thermal and Chemical Non-equilibrium**
- 6.0 Future Work for Phase II**
- References**

## 1.0 ACTIVITY SUMMARY

This is the Phase I final report, which summarizes our following R & D activities:

### 1.1 Development of a BGK-NS Solver for Magnetogasdynamics in Thermal and Chemical Equilibrium

Because of the time limitations of Phase I and the large amount of effort invested in the development of the gas-kinetic flow solver and the adjoint optimization method for weakly ionized hypersonic flows, we have focused on the development of a BGK-NS solver for magnetogasdynamics in thermal and chemical equilibrium in Phase I. This is a first step that will be further extended in Phase II. Section 2 discusses the governing equations of magnetogasdynamics in thermal and chemical equilibrium and the corresponding gas-kinetic BGK-NS solver.

### 1.2 Development of an Adjoint Optimization Method for Magnetogasdynamics in Thermal and Chemical Equilibrium

Based on the above BGK-NS solver, we have developed the corresponding discrete adjoint equations for the viscous, low magnetic Reynolds number approximation. These equations have been implemented into a preliminary adjoint solver which is capable of producing gradient information for arbitrary cost functions (unlike the continuous version of the adjoint) and for arbitrarily large numbers of design parameters with minimum cost (a flow solution and an adjoint solution only.) Details of this work are presented in Section 3.

### 1.3 Hypersonic Flow Past a Cylinder: Test Case

To validate the gas-kinetic BGK-NS solver and the adjoint optimization method, the hypersonic flow past cylinder case were numerically investigated and the results are presented in Section 4.

### 1.4 Development of BGK-Burnett Solver for Gas Dynamics in Thermal and Chemical Equilibrium

In addition, we will develop BGK-Burnett solver in Section 5 to explore the possibility of extending the approach beyond the continuum regime. In order to validate the resulting BGK-Burnett scheme, the plane Poiseuille flow will be numerically investigated.

### 1.5 Development of Gas-Kinetic Navier-Stokes Solver for Weakly Ionized Hypersonic Flows

In addition, we have also explored the possibility of extending the gas-kinetic CFD approach to weakly ionized hypersonic flows. Following an 11-species air model and the two-temperature model used in *LAURA* [1-2], a preliminary gas-kinetic equivalence of *LAURA* is presented in Section 6.

## 2.0 BGK-NS SCHEME FOR MAGNETOGASDYNAMICS IN THERMAL AND CHEMICAL EQUILIBRIUM

Our ultimate goal for this STTR project is to develop an adjoint optimization method for electromagnetic control of weakly ionized hypersonic flows. Due to the time limitations of Phase I and the large amount of initial effort involved in the development of an adjoint optimization method based on a gas-kinetic flow solver, however, we have first developed a gas-kinetic flow solver and an adjoint optimization method for magnetogasdynamics in thermal and chemical equilibrium. This will serve as the foundation for a further and more detailed generalization of the approach to weakly ionized hypersonic flows in Phase II.

### 2.1 Governing Equations

The equations governing a conducting flow in a magnetic field can be obtained by simply coupling the pre-Maxwell equation to the fluid conservation equations through the momentum and energy equations. The fluid conservation equations up to the Navier-Stokes order of the Chapman-Enskog expansion are

$$\begin{cases} \frac{\partial}{\partial t} \rho + \frac{\partial}{\partial x^j} (\rho U^j) = 0 \\ \frac{\partial}{\partial t} (\rho U^i) + \frac{\partial}{\partial x^j} (\rho U^i U^j + \delta^{ij} p - \tau^{ij}) = 0 \\ \frac{\partial}{\partial t} (\rho \varepsilon) + \frac{\partial}{\partial x^j} [(\rho \varepsilon + p) U^j - U^i \tau^{ij} - \kappa \frac{\partial T}{\partial x^j}] = 0 \end{cases} \quad (2-1)$$

Here  $\rho$ ,  $p$ ,  $T$ , and  $\varepsilon$  are the density, pressure, temperature, and the total energy respectively.  $U^i$  is the velocity component and  $\tau^{ij}$  is the shear stress.  $\kappa$  is the thermal conductivity coefficient.

In the presence of a magnetic field, a conducting fluid can generate a conduction current  $j^i$ , which may be computed by the pre-Maxwell equation

$$j^i = \varepsilon^{ijk} \frac{\partial}{\partial x^j} \left( \frac{B^k}{\mu_m} \right) \quad (2-2)$$

where  $B^k$  is the magnetic field and  $\mu_m$  is the magnetic permeability. To include the electromagnetic effects into (2-1), one should add the Lorentz force  $F_{em}^i = \varepsilon^{ijk} j^j B^k$  to the momentum equation and Joule heating  $P_{em} = E^i j^i$  to the total energy equation. Here  $E^i$  is the electric field, which may be computed by combining the pre-Maxwell equation of (2-2) and the Ohm's law:

$$E^i = \frac{j^i}{\sigma} - \varepsilon^{ijk} U^j B^k \quad (2-3)$$

where  $\sigma$  is the electrical conductivity. As a result, equations of (2-1) are generalized to

$$\begin{cases} \frac{\partial}{\partial t} \rho + \frac{\partial}{\partial x^j} (\rho U^j) = 0 \\ \frac{\partial}{\partial t} (\rho U^i) + \frac{\partial}{\partial x^j} (\rho U^i U^j + \delta^{ij} p - \tau^{ij}) = \varepsilon^{ijk} j^j B^k \\ \frac{\partial}{\partial t} (\rho \varepsilon) + \frac{\partial}{\partial x^j} [(\rho \varepsilon + p) U^j - U^i \tau^{ij} - \kappa \frac{\partial T}{\partial x^j}] = \frac{j^i j^i}{\sigma} - \varepsilon^{ijk} j^i U^j B^k \end{cases} \quad (2-4)$$

A conducting fluid in an imposed magnetic field can self induce a magnetic field. If the influence of the self-induced magnetic field is not negligible, one has to further add the magnetic induction equation, which is derived from Faraday's law, to (2-4)

$$\begin{cases} \frac{\partial}{\partial t} \rho + \frac{\partial}{\partial x^j} (\rho U^j) = 0 \\ \frac{\partial}{\partial t} (\rho U^i) + \frac{\partial}{\partial x^j} (\rho U^i U^j + \delta^{ij} p - \tau^{ij}) = \varepsilon^{ijk} j^j B^k \\ \frac{\partial}{\partial t} (\rho \varepsilon) + \frac{\partial}{\partial x^j} [(\rho \varepsilon + p) U^j - U^i \tau^{ij} - \kappa \frac{\partial T}{\partial x^j}] = \frac{j^i j^i}{\sigma} - \varepsilon^{ijk} j^i U^j B^k \\ \frac{\partial}{\partial t} B^i - (1 - \delta^{ij}) \frac{\partial}{\partial x^j} (U^i B^j - U^j B^i) = -(1 - \delta^{ij}) \frac{\partial}{\partial x^j} \left\{ \frac{1}{\sigma} \left[ \frac{\partial}{\partial x^i} \left( \frac{B^j}{\mu_m} \right) - \frac{\partial}{\partial x^j} \left( \frac{B^i}{\mu_m} \right) \right] \right\} \end{cases} \quad (2-5)$$

For multidimensional cases, there is another Maxwell's equation which acts as a constraint to the numerical algorithm

$$\frac{\partial B^i}{\partial x^i} = 0 \quad (2-6)$$

## 2.2 Gas-kinetic BGK-NS Scheme

There are several numerical algorithms available in the literature (e.g., [3-5]) for the solution of the governing equations of (2-5) based on the continuum CFD approach. In this project, we will develop a gas-kinetic CFD algorithm for the solution of the governing equations of (2-5). The gas-kinetic CFD approach has several advantages over the more widely used continuum CFD approach:

- Similar to DSMC, no macroscopic governing equation is needed before the construction of a gas-kinetic scheme. Since the macroscopic governing equations are derived from the gas-kinetic theory, a gas-kinetic CFD method can always satisfy the corresponding macroscopic governing equations automatically
  - The entropy condition is automatically satisfied
  - The scheme is positivity-preserving
  - The scheme is free of any sonic point glitch
  - The scheme is free of odd-even decoupling
- A gas-kinetic scheme treats the inviscid and viscous fluxes as a single entity. This makes its extension beyond the continuum regime much easier. Its integration with DSMC or Direct Boltzmann solvers in the rarefied flow regime is also much more straightforward than the continuum CFD approach.
- The numerical fluxes given by a gas-kinetic scheme are for all speeds. No preconditioning is needed for incompressible or hypersonic flows.

However, theoretically it is very difficult to construct an equilibrium state and a single kinetic transport equation to exactly recover the magnetogasdynamics equations of (2-5). Basically there is no corresponding "particle" picture to represent the magnetic field evolution. Therefore, we have to treat the

flow and magnetic fields differently. Whereas the flow field is treated with the gas-kinetic theory, the magnetic fluxes are split directly based on the macroscopic equation using the gas-kinetic theory as shown in [6].

The governing equations of (2-5) can be rewritten as

$$\frac{\partial Q}{\partial t} + \frac{\partial F}{\partial x} + \frac{\partial G}{\partial y} + \frac{\partial H}{\partial z} = S \quad (2-7)$$

with

$$Q = \begin{Bmatrix} \rho \\ \rho U \\ \rho V \\ \rho W \\ \rho \varepsilon \\ B_x \\ B_y \\ B_z \end{Bmatrix}, F = \begin{Bmatrix} \rho U \\ \rho U^2 + p - \tau_{xx} \\ \rho UV - \tau_{xy} \\ \rho UW - \tau_{xz} \\ (\rho \varepsilon + p)U - (U\tau_{xx} + V\tau_{xy} + W\tau_{xz}) - \kappa \frac{\partial T}{\partial x} \\ 0 \\ UB_y - VB_x \\ UB_z - WB_x \end{Bmatrix}, \dots \quad (2-8)$$

A finite-volume formulation of (2-7) with implicit treatment of the source term can be written as

$$\left[ \frac{1}{\Delta t} - \left( \frac{\partial S}{\partial Q} \right)_i^{\tilde{n}} \right] \Delta Q = - \frac{Q_i^{\tilde{n}} - Q_i^n}{\Delta t} - \sum_{l=i,j,k} \frac{\bar{F}_{l+1/2}^n A_{l+1/2}^n - \bar{F}_{l-1/2}^n A_{l-1/2}^n}{V_l} + S_i^{\tilde{n}} \quad (2-9)$$

Here  $\bar{F}$  is the numerical flux across a cell interface in the normal direction

$$\bar{F} = \begin{Bmatrix} \rho \bar{U} \\ \rho \bar{U}U + p n_x - \tau_{nx} \\ \rho \bar{U}V + p n_y - \tau_{ny} \\ \rho \bar{U}W + p n_z - \tau_{nz} \\ (\rho \varepsilon + p) \bar{U} - (U\tau_{nx} + V\tau_{ny} + W\tau_{nz}) - \kappa \frac{\partial T}{\partial s_n} \\ (Vn_y + Wn_z)B_x - U(B_y n_y + B_z n_z) \\ (Un_x + Wn_z)B_y - V(B_x n_x + B_z n_z) \\ (Un_x + Vn_y)B_z - W(B_x n_x + B_y n_y) \end{Bmatrix} \quad (2-10)$$

where  $\bar{U} = Un_x + Vn_y + Wn_z$ , and  $n$  represents the normal direction.

Now the problem that remains is how to compute the numerical flux across a cell interface. As mentioned earlier, the first five components of the flux of (2-10) are related to the flow field. Therefore, they can be computed by the gas-kinetic BGK-NS scheme in [7]. The BGK model can be written as

$$f_t + uf_x + vf_y + wf_z = \frac{g - f}{\tau} \quad (2-11)$$

where  $f$  is the gas distribution function and  $g$  is the equilibrium state approached by  $f$ . Both  $f$  and  $g$  are functions of space  $(x, y, z)$ , time  $t$ , particle velocities  $(u, v, w)$  and internal degrees of freedom  $\xi$ . The particle collision time  $\tau$  is related to the viscosity and heat conduction coefficient. The equilibrium state is a Maxwellian distribution

$$g = \rho \left( \frac{m}{2k\pi T} \right)^{\frac{3+N}{2}} \exp \left\{ -\frac{m}{2kT} [(u-U)^2 + (v-V)^2 + (w-W)^2 + \xi^2] \right\} \quad (2-12)$$

where  $m$  is the molecular weight,  $k$  is the Boltzmann constant,  $N$  is the total number of internal degrees of freedom, and  $\xi^2 = \sum_{n=1}^N \xi_n^2$ . The underlying assumption in the above equilibrium state is that each degree of freedom shares the same amount of internal energy  $kT/2$ , or the so-called equilibrium flow. The relation between the first five components of the conservative variable in (2-8) with the gas distribution function is

$$Q^F = \begin{Bmatrix} \rho \\ \rho U \\ \rho V \\ \rho W \\ \rho \varepsilon \end{Bmatrix} = \int \psi f d\Xi \quad (2-13)$$

where  $\psi$  is the vector of moments

$$\psi = \begin{Bmatrix} 1 \\ u \\ v \\ w \\ \frac{1}{2}(u^2 + v^2 + w^2 + \xi^2) \end{Bmatrix} \quad (2-14)$$

and  $d\Xi = dudvdwd\xi$  is the volume element in the phase space with  $d\xi = d\xi_1 \cdots d\xi_N$ . Since mass, momentum, and energy are conserved during the particle collisions,  $f$  and  $g$  satisfy the conservation constraint

$$\int (g - f) \psi d\Xi = 0 \quad (2-15)$$

at any point in space and time. The relation between the first five components of the fluxes in (2-8) with the gas distribution function is very similar. For example,

$$F^F = \begin{Bmatrix} \rho U \\ \rho U^2 + p - \tau_{xx} \\ \rho UV - \tau_{xy} \\ \rho UW - \tau_{xz} \\ (\rho \varepsilon + p)U - (U\tau_{xx} + V\tau_{xy} + W\tau_{xz}) - \kappa \frac{\partial T}{\partial x} \end{Bmatrix} = \int \psi u f d\Xi \quad (2-16)$$

The derivation of the Navier-Stokes equations from the BGK model can be found in [8].

Using (2-16), the first five components of the fluxes at the interface can be computed from the gas distribution function at the interface. The general solution of the BGK model gives the gas distribution function at a cell interface  $(x_{i+1/2}, y_j, z_k)$  and time  $t$  as

$$f(x_{i+1/2}, y_j, z_k, t, u, v, w, \xi) = \frac{1}{\tau_0} \int_0^t g(x', y', z', t', u, v, w, \xi) e^{-(t-t')/\tau} dt' + e^{-t/\tau} f_0(x_{i+1/2} - ut, y_j - vt, z_k - wt)$$

(2-17)

where  $x' = x_{i+1/2} - u(t - t')$ ,  $y' = y_j - v(t - t')$ , and  $z' = z_k - w(t - t')$  are the particle trajectory and  $f_0$  is the initial gas distribution function at the beginning of each time step ( $t = 0$ ). Two unknowns  $g$  and  $f_0$  in (2-17) must be specified in order to obtain the solution  $f$ . For simplicity, the directional splitting approach is adopted. Therefore, the one-dimensional notions and the notion of ( $x_{i+1/2} = 0, y_j = 0, z_k = 0$ ) will be used in the following text.

Based on the Chapman-Enskog expansion of the BGK model, the gas distribution function up to the Navier-Stokes order at the point  $x = 0$  and time  $t = 0$  has the form

$$f_{NS} = g - \tau \left( \frac{\partial g}{\partial t} + u \frac{\partial g}{\partial x} \right) \quad (2-18)$$

where  $\phi_1 = -\tau \left( \frac{\partial g}{\partial t} + u \frac{\partial g}{\partial x} \right)$  satisfies the compatibility condition  $\int \psi \phi_1 d\Xi = 0$ . To the second-order accuracy, the gas distribution function around the point  $x = 0$  at time  $t = 0$  can be approximated as

$$f_{NS} = g + \frac{\partial g}{\partial x} x - \tau \left( \frac{\partial g}{\partial t} + u \frac{\partial g}{\partial x} \right) \quad (2-19)$$

Therefore, given the initial discontinuous macroscopic variables at the left and right hand sides of a cell interface, the initial gas distribution function  $f_0$  has the form

$$f_0 = \begin{cases} g^l [1 + a^l x - \tau(a^l u + A^l)] & x \leq 0 \\ g^r [1 + a^r x - \tau(a^r u + A^r)] & x \geq 0 \end{cases} \quad (2-20)$$

It is noteworthy that the terms proportional to  $\tau$  in (2-20) represent the non-equilibrium parts of the Chapman-Enskog expansion. These non-equilibrium terms have no direct contribution to the macroscopic conservative variables, i.e.,

$$\begin{aligned} \int (a^l u + A^l) \psi g^l d\Xi &= 0 \\ \int (a^r u + A^r) \psi g^r d\Xi &= 0 \end{aligned} \quad (2-21)$$

which are also the equations used to determine  $A^l$  and  $A^r$ . On the other hand, they do affect the fluxes. In other words, the gas-kinetic BGK scheme has more information and gives a more realistic description of the viscous flows than the traditional continuum Navier-Stokes solvers.

Similarly, one can construct the equilibrium state  $g$  around ( $x = 0, t = 0$ ) as

$$g = g_0 [1 + (1 - H(x)) \bar{a}^l x + H(x) \bar{a}^r x + \bar{A} t] \quad (2-22)$$

where  $g_0$  is the value of the Maxwellian distribution function at ( $x = 0, t = 0$ ) and  $H(x)$  is the Heaviside function defined as

$$H[x] = \begin{cases} 0 & x \leq 0 \\ 1 & x \geq 0 \end{cases} \quad (2-23)$$

As shown in the following, all unknowns of  $a^l$ ,  $a^r$ ,  $A^l$ ,  $A^r$ ,  $\bar{a}^l$ ,  $\bar{a}^r$ , and  $\bar{A}$  in both (2-20) and (2-22) can be related to the derivatives of a Maxwellian in space and time.

The dependence of  $a^l$ ,  $a^r$ ,  $A^l$ ,  $A^r$ ,  $\bar{a}^l$ ,  $\bar{a}^r$ , and  $\bar{A}$  on the particle velocities can be obtained from a Taylor series expansion of a Maxwellian and has the following form

$$\begin{aligned}
a^l &= a_1^l + a_2^l u + a_3^l v + a_4^l w + a_5^l \frac{1}{2}(u^2 + v^2 + w^2 + \xi^2) = a_\alpha^l \psi_\alpha \\
A^l &= A_1^l + A_2^l u + A_3^l v + A_4^l w + A_5^l \frac{1}{2}(u^2 + v^2 + w^2 + \xi^2) = A_\alpha^l \psi_\alpha \\
&\vdots \\
\bar{A} &= \bar{A}_1 + \bar{A}_2 u + \bar{A}_3 v + \bar{A}_4 w + \bar{A}_5 \frac{1}{2}(u^2 + v^2 + w^2 + \xi^2) = \bar{A}_\alpha \psi_\alpha
\end{aligned} \tag{2-24}$$

where all coefficients  $a_1^l, a_2^l, \dots, \bar{A}_5^l$  are local constants.

After the reconstruction stage, one obtains the left and right hand side values of the conservative variables at the interface,  $Q_{i+1/2}^{F,l}$  and  $Q_{i+1/2}^{F,r}$ . With the relation of (2-13), the values of  $\rho^l, U^l, V^l, W^l, T^l$  and  $\rho^r, U^r, V^r, W^r, T^r$  in the Maxwellian distribution functions can be determined. Similarly,  $a^l$  and  $a^r$  can be computed by

$$\begin{aligned}
\int g^l a^l \psi d\Xi &= \frac{Q_{i+1/2}^{F,l} - Q_i^F}{x_{i+1/2} - x_i} \\
\int g^r a^r \psi d\Xi &= \frac{Q_{i+1}^F - Q_{i+1/2}^{F,r}}{x_{i+1} - x_{i+1/2}}
\end{aligned} \tag{2-25}$$

After determination of  $a^l$  and  $a^r$ ,  $A^l$  and  $A^r$  can be obtained by the compatibility condition of (2-21).

Moreover, according to [7], the values of  $\rho_0, U_0, V_0, W_0$ , and  $T_0$  in  $g_0$  can be determined by

$$\int g_0 \psi d\Xi = Q_0^F = \int_{u>0} g^l \psi d\Xi + \int_{u<0} g^r \psi d\Xi \tag{2-26}$$

Accordingly  $\bar{a}^l$  and  $\bar{a}^r$  can be computed by

$$\begin{aligned}
\int g_0 \bar{a}^l \psi d\Xi &= \frac{Q_0^F - Q_i^F}{x_{i+1/2} - x_i} \\
\int g_0 \bar{a}^r \psi d\Xi &= \frac{Q_{i+1}^F - Q_{i+1/2}^{F,r}}{x_{i+1} - x_{i+1/2}}
\end{aligned} \tag{2-27}$$

The only unknown left is  $\bar{A}$ , which can be found by the integration of the conservation constraint of (2-15) over the whole time step  $\Delta t$

$$\int_0^{\Delta t} \int (g - f) \psi dt d\Xi = 0 \tag{2-28}$$

After determination of the distribution function  $f$  at the cell interface, the first five components of the fluxes in (2-8) can be obtained through (2-16). We can also evaluate the heat flux across the cell interface

$$q = \frac{1}{2} \int (u - U) [(u - U)^2 + (v - V)^2 + (w - W)^2 + \xi^2] f d\Xi \tag{2-29}$$

In order to fix the problem of the fixed unit Prandtl number for the BGK solutions, the energy flux is modified to have the correct heat transfer through the cell interface,  $F_{\rho\epsilon}^{NEW} = F_{\rho\epsilon} + (1/\text{Pr} - 1)q$ . This completes our discussion of the discretization of the fluxes related to the flow field.

Next, we discuss how to compute the components of the fluxes related to the magnetic field. Let us use the flux component in the  $x$ -direction as an example. As shown above, in the gas-kinetic theory, the flux is associated with the particle motion across a cell interface. The splitting of the flux component in the  $x$ -direction is determined by the particle motion in this direction. Other quantities including the magnetic field can be considered as passive scalars which are transported with the  $x$ -direction particle velocity. For example, the density  $\rho$  can be split into

$$\rho^+ = \int_{u>0} g d\Xi = \rho \frac{1}{2} \operatorname{erfc}\left(-\sqrt{\frac{m}{2kT}} U\right) \equiv \rho \langle u^0 \rangle_+, \rho^- = \int_{u<0} g d\Xi = \rho \frac{1}{2} \operatorname{erfc}\left(\sqrt{\frac{m}{2kT}} U\right) \equiv \rho \langle u^0 \rangle_- \quad (2-30)$$

Any macroscopic quantity  $Z$  without explicitly containing the  $x$ -component velocity  $U$ , including the magnetic field  $B_x$ ,  $B_y$ , and  $B_z$ , can be split in a similar way

$$Z^+ = Z \langle u^0 \rangle_+, Z^- = Z \langle u^0 \rangle_- \quad (2-31)$$

The above relations mean that the quantity  $Z$  is simply advected with the particle transport in the  $x$ -direction.

On the other hand, the  $x$ -direction momentum  $\rho U$  can be split into

$$\begin{aligned} (\rho U)^+ &= \int_{u>0} u g d\Xi = \rho [U \langle u^0 \rangle_+ + \frac{1}{2} \frac{\exp(-\frac{m}{2kT} U^2)}{\sqrt{\frac{m}{2kT}} \pi}] \equiv \rho \langle u^1 \rangle_+ \\ (\rho U)^- &= \int_{u<0} u g d\Xi = \rho [U \langle u^0 \rangle_- - \frac{1}{2} \frac{\exp(-\frac{m}{2kT} U^2)}{\sqrt{\frac{m}{2kT}} \pi}] \equiv \rho \langle u^1 \rangle_- \end{aligned} \quad (2-32)$$

Similarly, any quantity containing the  $U$  term, including  $UB_x$ ,  $UB_y$ , and  $UB_z$ , can be split as

$$(ZU)^+ = Z \langle u^1 \rangle_+, (ZU)^- = Z \langle u^1 \rangle_- \quad (2-33)$$

For the magnetic field, the above splitting implies that the field is frozen into the particle motion and transported with the fluid.

As a result, the last three components of the fluxes in (2-8), which are related to the magnetic field, can be computed by

$$F^B = \begin{Bmatrix} 0 \\ UB_y - VB_x \\ UB_z - WB_x \end{Bmatrix} = (F^B)^+ + (F^B)^- \quad (2-34)$$

The positive flux is

$$(F^B)^+ = \begin{Bmatrix} 0 \\ B_y \langle u^1 \rangle_+ - B_x V \langle u^0 \rangle_+ \\ B_z \langle u^1 \rangle_+ - B_x W \langle u^0 \rangle_+ \end{Bmatrix} \quad (2-35)$$

and the negative flux is

$$(F^B)^- = \begin{Bmatrix} 0 \\ B_y \langle u^1 \rangle_- - B_x V \langle u^0 \rangle_- \\ B_z \langle u^1 \rangle_- - B_x W \langle u^0 \rangle_- \end{Bmatrix} \quad (2-36)$$

Finally, we will discuss how to numerically enforce the divergence free condition of (2-6) for the magnetic field. A common approach is to use a correction method, in which a Poisson equation for the potential  $\phi$

$$\frac{\partial^2 \phi^j}{\partial x^i \partial x^i} + \frac{\partial B^j}{\partial x^j} = 0 \quad (2-37)$$

is solved and the corrected magnetic field  $B_c^i$  is obtained through

$$B_c^i = B^i + \frac{\partial \phi}{\partial x^i} \quad (2-38)$$

where  $\frac{\partial B_c^i}{\partial x^i} = 0$  is satisfied.

### 3.0 ADJOINT OPTIMIZATION METHOD FOR MAGNETOGASDYNAMICS IN THERMAL AND CHEMICAL EQUILIBRIUM

The main objective of this program is to develop and implement viable approaches for the design optimization of magnetogasdynamics problems. To further clarify this objective, we intend to develop a method that enables us to predict the sensitivity/gradient of arbitrary cost (and constraint) functions to very large numbers of design parameters with reasonable computational cost. At the moment, we have allowed design parameters of two separate kinds, although other parameters can be included since the formulation is entirely generic:

- **Vehicle shape:** parametric design changes to a baseline geometry that, through the effect of boundary conditions on the flow, can dramatically change the functions of interest.
- **Applied electric and magnetic fields:** the strengths and shape of these fields can have a significant impact on the functions of interest. Furthermore, conductivity and permittivity distributions can also impact the values of the functions of interest and may require a very large number of parameters to be appropriately described.

A basic requirement of our approach is that the (cost) functions of interest (which may be either cost functions for the optimization or constraint functions that the optimization problem must satisfy) can be arbitrary functions of the flow solution/state variables. In our early work we have tackled the drag coefficient of the body and the integrated heat flux through the wall as basic cost functions, but the methodology allows for any other function to be included with a very small development cost, namely, the computation of the partial derivative of this function with respect to the state vector linearized about the solution provided by the flow solver.

With this in mind we have developed a method that can easily provide derivatives of each of these functions with respect to arbitrary numbers of design parameters (appropriately chosen by the designer) with a cost which is equivalent to two flow solutions: a traditional flow solution followed by an adjoint solution which is of very similar cost to the flow solution (in terms of CPU and memory requirements.) This cost is for the derivative of a *single* cost function with respect to a large number of design parameters. If the gradients/sensitivities of additional functions are required, the flow solution may be reused, but additional adjoint solutions (one per function) must be carried out to obtain the necessary gradients. Note, however, that the treatment of additional functions does not require the development of an entirely different adjoint solver (this misconception is common in our community): it simply requires that a new right hand side (one could call this a forcing vector) be developed. As mentioned above the cost of this is truly minimal.

After careful examination of the governing equations of the problem (see Section 2.1) the choice was made to develop **discrete adjoint equation** sets for the N-S low magnetic Reynolds number approximation in Eq. (26) of Ref. [3]. This choice was justified due to the extreme similarity of the equations with the Navier-Stokes equations of fluid flow, for which we have built up considerable experience through the years.

Several key choices in the development have also been made. These choices make this program unique in comparison with previous efforts in our group at Stanford University. In particular, we have chosen to:

1. Use the *discrete adjoint equations* (rather than the continuous formulation) for the equations of magnetogasdynamics.

2. Develop a stand-alone, unstructured, discrete adjoint solver for the magnetogasdynamics equations.
3. Choose the "discretization" used in the discrete adjoint formulation. This "discretization" refers to the basic discretization for which the adjoint equations have been developed.

These are fundamental choices can strongly impact the usability and versatility of the resulting method and, therefore, details on the rationale for these choices is provided below after a short description of the discrete adjoint method.

### 3.1 Discrete Adjoint Equations

The conceptual derivation of the discrete adjoint equations for any system of governing equations is straightforward and is outlined in this section. We consider the problem of the minimization of an arbitrary cost function of interest,  $J(U, \beta)$ , which involves the solution,  $U$ , to a particular version of the magnetogasdynamics equations and a possibly large set of parameters,  $\beta$ , that may include various things such as the shape of the body, the parametric strength of imposed magnetic and electric fields, and possibly, the location and strength of energy addition. The changes in  $U$  that result from changes in  $\beta$  are not arbitrary since they must satisfy the governing equations of the magnetogasdynamics problem,  $N(U, \beta) \equiv N(U, X(\beta)) = 0$ , where  $X$  represents the mesh that may (or may not) change as a result of the changes in the design parameters  $\beta$  through a suitable mesh deformation procedure. The total derivatives of the cost function and governing equations can be represented as follows

$$\begin{aligned} \left[ \frac{dJ}{d\beta} \right] &= \left[ \frac{\partial J}{\partial U} \right] \left[ \frac{dU}{d\beta} \right] + \left[ \frac{\partial J}{\partial \beta} \right] \\ \left[ \frac{\partial N}{\partial U} \right] \left[ \frac{dU}{d\beta} \right] + \left[ \frac{\partial N}{\partial \beta} \right] &= 0 \end{aligned} \quad (3-1)$$

If we solve the adjoint equation  $\left[ \frac{\partial N}{\partial U} \right]^T v = \left[ \frac{\partial J}{\partial U} \right]^T$ , where  $v$  is the adjoint variable, we can find the derivatives of the cost function as

$$\left[ \frac{dJ}{d\beta} \right] = - \left[ \frac{\partial N}{\partial \beta} \right]^T v^T + \left[ \frac{\partial J}{\partial \beta} \right]. \quad (3-2)$$

Note that the adjoint equation does not depend on  $\beta$ . It only has to be solved once for each cost function  $J$ . The derivatives of the cost function in Eq. (3-2) no longer involve  $\frac{dU}{d\beta}$  and therefore can be

calculated without re-computing the solution to the governing equations. This is the key advantage of the adjoint method. For systems with few cost functions and many parameters/design variables the discrete adjoint approach outlined here is the most efficient alternative to obtain the sensitivities of a given function of interest. Notice that all of the expressions above are discrete versions involving vectors of very large dimensions and very large and sparse matrices (since the discretization stencils for the flow solver tend to be somewhat compact.) In order to develop the discrete adjoint equations one needs to come up with expressions for  $\left[ \frac{\partial N}{\partial U} \right]$  and  $\left[ \frac{\partial J}{\partial U} \right]$  for the discrete versions of  $N$ ,  $J$ , and  $U$ . These

expressions must take into account the actual discretization of the governing equations and the cost function. Although the development of these expressions can be lengthy and laborious, it amounts to

Careful application of the chain rule of differentiation to the actual discretization stencil chosen for the system solution.

All of the expressions for the adjoint equation (the main matrix,  $\left[\frac{\partial N}{\partial U}\right]$  with the boundary conditions that are included in it and the right hand side vectors  $\left[\frac{\partial J}{\partial U}\right]$  for the two cost functions described earlier have been developed, implemented and tested (see Section 3.4) including the inviscid and viscous terms of the residual  $N$ , a first-order discretization of the artificial dissipation fluxes, and the source terms for the momentum and energy equations that result from the Lorentz force and Joule heating. At present, the only limitation of this discrete adjoint implementation is that the variations of the eddy viscosity with respect to the flow solution have been neglected. This is a typical approach followed when the continuous adjoint formulation is used as it is impossible to analytically derive these expressions. In our case, it is simply a matter of additional derivations that have not been completed yet.

The solution of the adjoint equation

$$\left[\frac{\partial N}{\partial U}\right]^T v = \left[\frac{\partial J}{\partial U}\right]^T \quad (3-3)$$

is achieved using a matrix-free, ILU(0) preconditioned GMRES algorithm. Since Eq. (3-3) is a large linear system, GMRES has proven to be one of the most robust solvers for this type of problem. We have chosen to use a matrix-free version (in other words, we never store, even in sparse format, the matrix  $\left[\frac{\partial N}{\partial U}\right]$  or its transpose in order to avoid memory storage penalties. Although for the small test problems that we have used this memory penalty is not truly significant and does not hamper our efforts, for larger computations it may become a significant problem. Instead, we recomputed, on-the-fly, the terms in  $\left[\frac{\partial N}{\partial U}\right]$  for every iteration of the GMRES algorithm. Alternative compromises between storage and re-computation (for some of the most expensive terms) will be explored in Phase II. In addition, we will enhance the performance of the discrete adjoint solver by using improved preconditioning techniques and optimized implementations of the functions that calculate the various Jacobian terms of  $\left[\frac{\partial N}{\partial U}\right]$ .

### 3.2 Discrete vs. Continuous Adjoint Equations

Since most of our efforts at Stanford University (Alonso, Jameson, Reuther, et al.) have focused on the development of continuous adjoint formulations of the Reynolds-Averaged Navier-Stokes equations it is appropriate to discuss in this section the rationale that led us to the choice of a discrete adjoint approach for the equations of magnetogasdynamics. The various choices were based on the suitability (and generality) for long term efforts in magnetogasdynamics.

Several key reasons have led us to the decision to use a discrete formulation of the adjoint equations:

- A discrete formulation allows for the choice of arbitrary cost functions that will be needed to properly pose generic magnetogasdynamics optimization problems. In contrast, the continuous

adjoint approach will not allow proper treatment of all choices of cost functions, thus limiting the usability of the resulting method.

- The derivation of the continuous adjoint approach that includes all of the necessary variations (turbulence models, electrical conductivity, permeability, etc) was attempted but led to a very high-level of complexity unless some of these variations were neglected. In closely coupled problems in magnetogasdynamics, we felt that neglecting some interactions between the flow field and the magnetic/electric fields would lead to erroneous results. The discrete approach accounts for these variations.
- The derivatives produced by the discrete method are in agreement with the discrete computations of the system solution.

### 3.3 Discretization Choices for the Discrete Adjoint Equations

The resulting discrete adjoint equations depend on the discretization approach chosen for the residuals of the governing equations. Previous experience in the continuous adjoint area ([28]) has shown that one may choose consistent discretizations of the governing equations and the adjoint equations separately with minimal errors for reasonably-sized meshes. For this reason, our discrete adjoint solver is based on a finite-volume, second-order accurate discretization of the governing equations of the flow. Although this discretization is different from the BGK approach used in the flow solver, the sensitivity information must be consistent in the limit of small mesh sizes. Since the eigenvalues of the flow linearization and of the adjoint equations are identical, the only requirement on the choice of discretization is that it be stable so that the adjoint solver can be made to converge ([27]).

With these choices for the discrete adjoint solver, we believe that we are in a position to tackle the difficult problem of magnetogasdynamics design regardless of the flow solver and discretization used and for any choice of cost function and design parameterization that can involve more than simple changes to the physical shape of the geometry. This will not be the case if alternative approaches to the formulation of the adjoint system (for example, the continuous version) are employed.

### 3.4 Sample Sensitivity and Convergence Histories of the Discrete Adjoint Implementation

The procedure outlined above has been implemented into a stand-alone discrete adjoint solver for the low magnetic Reynolds number approximation of the magnetogasdynamics equations. As mentioned above, the discrete adjoint solver includes all of the necessary terms:

- Inviscid fluxes.
- Viscous fluxes (with “frozen” eddy viscosity.)
- First-order artificial dissipation fluxes.
- Source terms (for both the Lorenz force and Joule heating.)

In addition to these terms that are part of the  $\left[\frac{\partial \mathcal{N}}{\partial \mathcal{U}}\right]^T$  operator, we have developed right hand side

approximations for the  $\left[\frac{\partial \mathcal{J}}{\partial \mathcal{U}}\right]^T$  terms for two different cost functions,  $\mathcal{J}$ , namely the coefficient of drag of the body and the integrated heat transfer through the (constant temperature) wall. Additional cost functions can be easily derived and implemented as another right-hand-side for the adjoint solver.

The ultimate use of the adjoint solution  $\nu$  is to include it in Eq. (3-2) to compute the total derivative of a cost function  $J$  with respect to the design parameters  $\beta$ . The ability to compute these derivatives accurately is the main validation step of an adjoint solution approach. The configuration used as a preliminary test case is taken from Ref. [3]. It consists of a blunt cylinder immersed in an incoming flow with a Mach number of 16 aligned with the axis of symmetry of the cylinder. A typical flow solution (obtained with a finite volume implementation of the low magnetic Reynolds number approximation in the parallel, multiblock-structured, Stanford University code, TFLO2000) can be seen in Fig. 3.1 below.

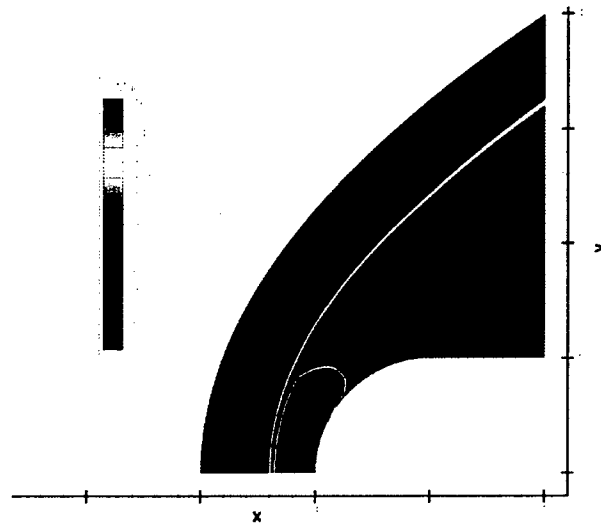


**Figure 3-1 Mach Number Contours for the Flow Around a Blunt Cylinder at a Zero Angle of Attack. Baseline Solution for Discrete Adjoint Calculation.**

Based on the baseline solution in Fig 3-1, we computed discrete adjoint solutions for both the coefficient of drag and heat transfer cost functions described earlier. The robustness of the preconditioned GMRES implementation can be seen in Fig 3-2 below where the convergence history of the discrete adjoint solution (with  $J$  being the coefficient of drag) is shown. In less than 6000 residual evaluations, corresponding to approximately 400 GMRES iterations, the adjoint equation has converged over 3-4 orders of magnitude (the various graphs denote the convergence histories of the adjoint variables for the mass, momentum, energy, and turbulent kinetic energy and dissipation rate equations. Previous studies for the Navier-Stokes equations ([29],[30]) have shown that this convergence level in the adjoint solution is more than adequate. In fact, a level of convergence of 2 orders of magnitude has been found to be sufficient for accurate gradient information to be obtained. The first portion of the convergence history (labeled I) shows the convergence for a mesh that has been coarsened (by taking every other point) in each coordinate direction. After a certain level of convergence is obtained, the fine mesh (128 x 96 x 16 cells in the streamwise, normal, and azimuthal directions) is started (labeled II in the Fig.) and convergence proceeds.

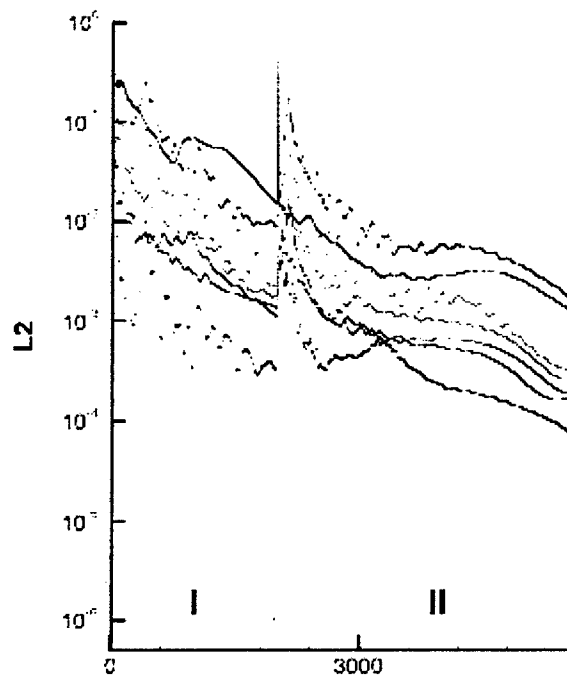


**Figure 3-2 Discrete Adjoint Solver Convergence for the Baseline Solution in Fig 3-1 in Both the Fine (II) and First Level Coarse (I) meshes.**

Using Eq. 3-2, we can use this adjoint solution (and an equivalent one obtained for  $J$  being the heat transfer measure) to compute and validate the gradients with respect to design parameters  $\beta$  of interest. Following the types of design parameters that we have mentioned earlier, we present, in Table 3-1 below, the results of the comparison of the discrete-adjoint-based gradient with those obtained by finite-differences of the original flow solver. Two types of parameters are considered: those related to the strength and location of the magnetic field and those related to the shape of the body itself. For the magnetic field design variables, we consider two design parameters: the strength of a dipole and its location. For the shape functions, we distributed 10 Hicks-Henne ([30]) "bump" functions evenly spaced from the stagnation point location to the end of the spherical portion of the body. The results for the first and last Hicks-Henne bump functions are reported here. All results are within 1-5% of the finite difference values of the sensitivities (appropriately non-dimensionalized.) We are currently looking into the cause of these differences but they are entirely expected as the exact equivalence can only be obtained when the finite difference gradients are exact (depending on the choice of step size) and when all of the terms in the governing equations are taken into account when computing the  $\left[ \frac{\partial N}{\partial U} \right]^T$  operator. As mentioned earlier we are currently using a first-order approximation to the artificial dissipation fluxes in the discrete adjoint solver and the eddy viscosity field is "frozen".

	Cost Functions, $J$					
	$C_D$			Integrated Heat Transfer		
	Adjoint	Finite Diff.	Rel. Error %	Adjoint	Finite Diff.	Rel. Error %
Bump 1	3.3227	3.3789	1.66	37.3885	35.6723	4.81
Bump 10	0.3422	0.3455	0.95	4.7523	4.6676	1.81
Dipole Strength	10.7588	11.2377	4.26	26.3412	27.0301	2.55
Dipole Position	2.1577	2.1553	1.11	7.5962	8.0345	5.45

**Table 3-1 Validation of Sensitivities Using Discrete Adjoint Solver**

We are currently conducting more extensive sensitivity validation numerical experiments and providing the computed sensitivities to the SNOPT non-linear constrained gradient-based optimizer to demonstrate the use of our adjoint methodology to simple design problems. We expect to present these results at the time of our final presentation at the end of June 2005.

#### 4.0 BGK-BURNETT SCHEME FOR GAS DYNAMICS IN THERMAL AND CHEMICAL EQUILIBRIUM

The BGK-NS solver developed above may be insufficient for hypersonic applications. This is mainly because a space vehicle may operate in a high-speed and low-density environment, in which the rarefaction effects are not negligible. A key measure of the rarefaction effects is the Knudsen number  $K_n$ , the ratio of the mean free path to the characteristic length. The higher the Knudsen number is, the more important the rarefaction effects become. During their atmospheric reentry, the freestream Knudsen numbers of both HITEN and Magellan spacecrafts range from 2 to 6.3 [9], indicating that the flowfield is in the transitional regime. In the flowfield around Reaction Control System (RCS), which will be used on future Reusable Launch Vehicles (RLV) and planetary probes, the Knudsen number varies from much less than one to greater than one from the continuum jet, through the interaction region and into the rarefied freestream [10]. The accurate simulation of these mixed continuum and rarefied flows calls for a computational algorithm, which can cover all continuum, transitional and rarefied flow regimes, or at least can cover the Knudsen number up to one. Such a need is further emphasized by the difficulty of simulating low-density, high-enthalpy flows around space vehicles on the ground-based facilities.

To extend our gas-kinetic scheme beyond the continuum regime, instead of truncating the Chapman-Enskog expansion of the BGK model at the Navier-Stokes order in (2-18), we keep the Chapman-Enskog expansion of the BGK model up to the Burnett order

$$f_{\text{Burnett}} = g - \tau Dg + \tau D(\tau Dg) \quad (4-1)$$

where  $D = \frac{\partial}{\partial t} + u \frac{\partial}{\partial x}$ . Since we are going to develop a scheme for the local time evolution around a cell interface, the variation of the collision time  $\tau$  around a cell interface within a time step is ignored. Therefore, the equation of (4-1) can be rewritten as

$$f_{\text{Burnett}} = g - \tau Dg + \tau^2 D^2 g \quad (4-2)$$

where  $\phi_2 = \tau^2 D^2 g$  satisfies the compatibility condition  $\int \psi \phi_2 d\Xi = 0$ . Note that the spatial and temporal variation of  $\tau$  at different numerical cells and different time steps are still accounted in the current BGK-Burnett scheme by changing  $\tau$  from cell to cell according to the viscosity coefficient and local pressure.

To third-order accuracy, the gas distribution function around the point  $x=0$  at time  $t=0$  can be approximated as

$$f_{\text{Burnett}} = g + \frac{\partial g}{\partial x} x + \frac{1}{2} \frac{\partial^2 g}{\partial x^2} x^2 - \tau \left( \frac{\partial g}{\partial t} + u \frac{\partial g}{\partial x} \right) - \tau \left( \frac{\partial^2 g}{\partial t \partial x} + u \frac{\partial^2 g}{\partial x^2} \right) x + \tau^2 \left( \frac{\partial^2 g}{\partial t^2} + 2u \frac{\partial^2 g}{\partial t \partial x} + u^2 \frac{\partial^2 g}{\partial x^2} \right) \quad (4-3)$$

Therefore, given the initial discontinuous macroscopic variables at the left and right hand sides of a cell interface, the initial gas distribution function  $f_0$  has the form

$$f_0 = \begin{cases} g^l \{ 1 + a^l x + \frac{1}{2} b^l x^2 - \tau [a^l u + A^l + (C^l + b^l u)x] + \tau^2 (B^l + 2u C^l + b^l u^2) \}, & x \leq 0 \\ g^r \{ 1 + a^r x + \frac{1}{2} b^r x^2 - \tau [a^r u + A^r + (C^r + b^r u)x] + \tau^2 (B^r + 2u C^r + b^r u^2) \}, & x \geq 0 \end{cases} \quad (4-4)$$

The values of  $\rho^l, U^l, V^l, W^l, T^l$  and  $\rho^r, U^r, V^r, W^r, T^r$  in the Maxwellian distribution functions, and  $a^l, a^r$  are computed in the same way as in the BGK-NS scheme. The new unknowns  $b^l$  and  $b^r$  can

be determined from

$$\begin{aligned}\int g^l b^l \psi d\Xi &= \left(\frac{\partial^2 Q}{\partial x^2}\right)_{i+1/2}^l \\ \int g^r b^r \psi d\Xi &= \left(\frac{\partial^2 Q}{\partial x^2}\right)_{i+1/2}^r\end{aligned}\quad (4-5)$$

After determination of  $a^l$ ,  $a^r$  and  $b^l$ ,  $b^r$ ,  $A^l$  and  $A^r$  are still obtained by the compatibility condition of (2-21). The new unknowns  $C^l$  and  $C^r$  can be determined by the compatibility condition

$$\begin{aligned}\int (b^l u + C^l) \psi g^l d\Xi &= 0 \\ \int (b^r u + C^r) \psi g^r d\Xi &= 0\end{aligned}\quad (4-6)$$

and  $B^l$ ,  $B^r$  further by the compatibility condition

$$\begin{aligned}\int (b^l u^2 + 2u C^l + B^l) \psi g^l d\Xi &= 0 \\ \int (b^r u^2 + 2u C^r + B^r) \psi g^r d\Xi &= 0\end{aligned}\quad (4-7)$$

Similarly, one can construct the equilibrium state  $g$  around  $(x=0, t=0)$  as

$$g = g_0 \left[ 1 + (1 - H(x)) \left( \bar{a}^l x + \frac{1}{2} \bar{b}^l x^2 \right) + H(x) \left( \bar{a}^r x + \frac{1}{2} \bar{b}^r x^2 \right) + \bar{A}t + \frac{1}{2} \bar{B}t^2 + \bar{C}xt \right] \quad (4-8)$$

The unknowns in (4-8) can be determined in a similar way as above.

Next, we first test our BGK-Burnett scheme for the Poiseuille flow under the external forcing term with the Knudsen number  $K_n = 0.1$ . As pointed out by many authors [11-14], even for this simple case with relative small gradient and Knudsen number, the Navier-Stokes equations fail to predict qualitatively correct solution. Specifically, for the external force driven case, the Navier-Stokes equations fail to reproduce the central minimum in the temperature profile and a non-constant pressure profile in the cross-stream direction, which are both predicted by the gas kinetic theory and observed in the DSMC results. Furthermore, based on the Navier-Stokes equations, it is impossible to correct this failure by modifying the equation of state, transport coefficient or boundary conditions. Unlike the slip phenomena, the discrepancy is not just near a boundary but throughout the system. The similar discrepancy is also happening for the pressure-driven case.

The setup of the external force driven case is given as follows [15-16]. The simulation fluid is a hard sphere gas with particle mass  $m=1$  and diameter  $d=1$ . At the reference density of  $\rho_0 = 1.21 \times 10^{-3}$ , the

mean free path is  $l_0 = \frac{m}{\sqrt{2}\pi\rho_0 d^2} = 186$ . The distance between the thermal walls is  $L_y = 10l_0$  and their

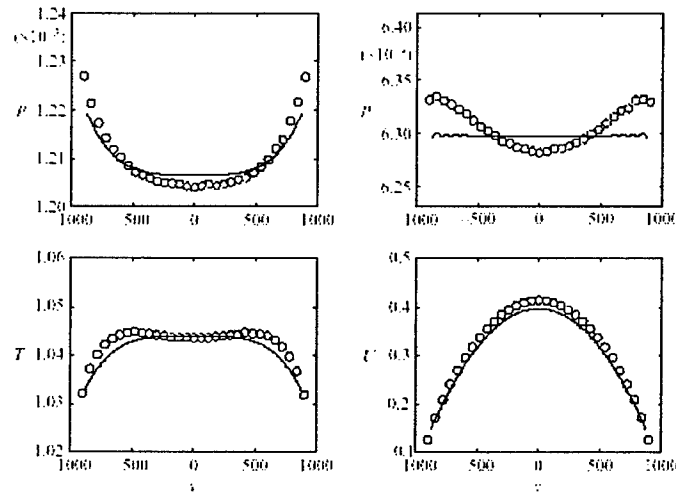
temperature is  $T_0 = 1$ . The reference fluid speed is  $U_0 = \sqrt{\frac{2kT_0}{m}} = 1$ , so the Boltzmann constant is taken

as  $k = \frac{1}{2}$ . The reference sound speed is  $c_0 = \sqrt{\frac{\gamma k T_0}{m}} = 0.91$  with  $\gamma = \frac{5}{3}$  for a monatomic gas. The

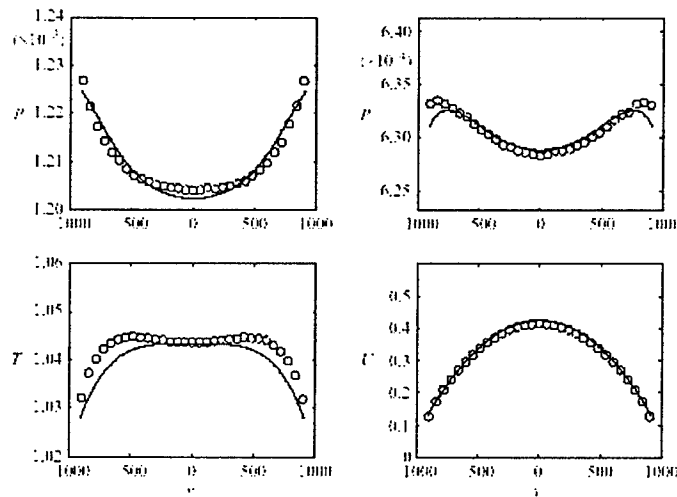
reference pressure is  $p_0 = \frac{\rho_0 k T_0}{m} = 6.05 \times 10^{-4}$ . The acceleration and pressure gradient are chosen so that the flow will be subsonic, laminar, and of similar magnitude in the two cases. Specifically,

$\rho_0|\vec{f}| = 8.31 \times 10^{-8}$  for the acceleration-driven case and  $\frac{dp}{dx} = 1.08 \times 10^{-7}$  for the pressure-driven case ( $p_+ = 1.5p_0$ ,  $p_- = 0.5p_0$ ,  $L_x = 30l_0$ ). In both cases, the Knudsen number is 0.1 and the Reynolds number is of order one. In all calculations, the cell size is half the mean free path of the initial data.

Figure 4-1(a) presents the results for the force-driven case in the cross-stream direction using the above BGK-NS scheme with the slip kinetic boundary condition. The circles in Figure 4-1(a) are the well-verified DSMC results [16]. Although the BGK-NS scheme is an accurate Navier-Stokes solver, even with the slip boundary condition, the predicted pressure distribution is constant in the cross-stream direction, which is different from the DSMC solution. In [16], a different Navier-Stokes solver is used. Both Navier-Stokes solvers give qualitatively similar results. In order to resolve the discrepancy between the Navier-Stokes and DSMC solutions, the gas-kinetic BGK-Burnett scheme is used. Figure 4-1(b) presents the BGK-Burnett results. It is found that the curved pressure distribution in the cross-stream direction is captured well. So, up to the Burnett order, the non-constant pressure distribution can be obtained. This is consistent with the analysis in [13].



(a) BGK-NS vs DSMC



(b) BGK-Burnett vs DSMC

**Figure 4-1 Flow distribution in the cross-stream direction for the external force-driven case  
(o DSMC results, — BGK results)**

In order to further validate the BGK-Burnett approach, we have calculated the mass flow rate through the channel for the pressure-driven Poiseuille flow. Both BGK-NS and BGK-Burnett schemes are used in the current calculations. The normalized mass flow rates are defined by  $\frac{Q}{\rho U^* h}$ , where  $Q$  is the mass flow

rate and  $\rho U^* h$  is the normalization factor. The velocity  $U^*$  is defined by  $U^* = \alpha \sqrt{\frac{2kT}{m}}$ , where  $\alpha$  is

related to the pressure gradient in the channel  $p = p_0(1 + \frac{\alpha x}{h})$  and  $h$  is the channel width. The calculated

solutions, as well as the analytical solution of [17], are shown in Figure 4-2. From this figure, we can clearly see the improvement of the BGK-Burnett solution over the BGK-NS solution. For most micro-channel flows in the laboratory, such as the experiments in [18], the highest Knudsen number at the outlet is about 0.2. Therefore, in the flow regime of these experiments, the slip Navier-Stokes equations are capable of capturing the physical solution. However, as the Knudsen number increases, such as up to 0.5, the BGK-Burnett scheme should be a more appropriate numerical method than the BGK-NS solver.

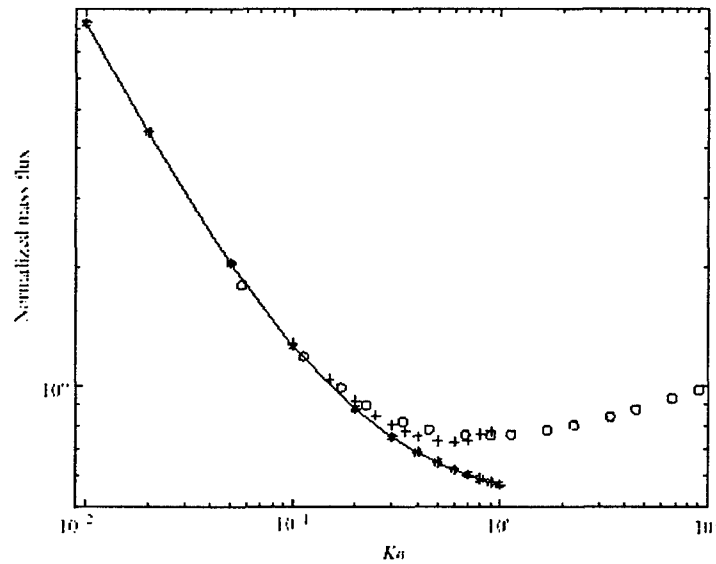


**Figure 4-2 Relation of the normalized mass flow rate versus Knudsen number for Poiseuille flow (o Boltzmann solution, x- BGK-NS, + BGK-Burnett)**

## 5.0 GENERALIZATION OF GAS-KINETIC NS SOLVER TO HYPERSONIC FLOWS IN THERMAL AND CHEMICAL NON-EQUILIBRIUM

Next, we discuss how to generalize the above BGK-NS scheme to hypersonic flows in thermal and chemical non-equilibrium. As a first step, a simpler Kinetic Flux Vector Splitting (KFVS) scheme is constructed here for the governing equations adopted by a widely used hypersonic CFD code, *LAURA*.

According to [1-2], the governing equations solved by *LAURA* can be written as

$$\begin{cases} \frac{\partial}{\partial t} \rho_s + \frac{\partial}{\partial x^j} (\rho_s U^j - \rho D_s \frac{\partial y_s}{\partial x^j}) = \dot{\omega}_s \\ \frac{\partial}{\partial t} (\rho U^i) + \frac{\partial}{\partial x^j} (\rho U^i U^j + \delta^{ij} p - \tau^{ij}) = 0 \\ \frac{\partial}{\partial t} (\rho \varepsilon) + \frac{\partial}{\partial x^j} [(\rho \varepsilon + p) U^j - \rho \sum_{s=1}^{N_t} (h_s D_s \frac{\partial y_s}{\partial x^j}) - U^i \tau^{ij} - \kappa \frac{\partial T}{\partial x^j} - \kappa_v \frac{\partial T_v}{\partial x^j}] = 0 \\ \frac{\partial}{\partial t} (\rho \varepsilon_v) + \frac{\partial}{\partial x^j} [\rho \varepsilon_v U^j - \rho \sum_{s=mol.} (h_{v,s} D_s \frac{\partial y_s}{\partial x^j}) - \kappa_v \frac{\partial T_v}{\partial x^j}] = \dot{\omega}_v \end{cases} \quad (5-1)$$

Here  $\rho_s$ ,  $D_s$ ,  $y_s$ ,  $\dot{\omega}_s$ ,  $h_s$ , and  $h_{v,s}$  are the density, effective diffusion coefficient, mole fraction, the mass production rate due to chemical reactions, enthalpy per unit mass, and vibrational-electronic enthalpy per unit mass for species  $s$  respectively. A 11-species air model (N, O, N<sub>2</sub>, O<sub>2</sub>, NO, N<sup>+</sup>, O<sup>+</sup>, N<sub>2</sub><sup>+</sup>, O<sub>2</sub><sup>+</sup>, NO<sup>+</sup>, and e<sup>-</sup>) is used in *LAURA*. A common velocity  $U^i$  is assumed for all species. To account for thermal non-equilibrium, a two-temperature model is used, in which the translational and rotational energy modes are assumed in equilibrium at the translational temperature  $T$ , and the vibrational, electronic, and electron translational energy modes are assumed in equilibrium at the vibrational temperature  $T_v$ .  $\rho$ ,  $p$ ,  $\tau^{ij}$ ,  $\varepsilon$ ,  $\varepsilon_v$ ,  $\kappa$  and  $\kappa_v$  are the density, pressure, shear stress, total energy per unit mass, vibrational-electronic energy per unit mass, frozen thermal conductivity for translational-rotational energy, and frozen thermal conductivity for vibrational-electronic energy for the gas mixture respectively.  $\dot{\omega}_v$  represents the vibrational-electronic energy production rate due to particle collisions. A detailed description of the governing equations of (5-1), including thermodynamic relations and chemical kinetic models, is referred to [1-2].

A finite-volume formulation of (5-1) with implicit treatment of the source term is the same as (2-9) in the form. The only problem left is how to construct KFVS scheme for computation of the numerical fluxes of (5-1) at the interfaces. In order to recover the governing equations of (5-1), 11 BGK models are needed such that each species satisfies its own BGK model

$$\frac{\partial f_s}{\partial t} + u_s^j \frac{\partial f_s}{\partial x^j} = \frac{g_s - f_s}{\tau_s} \quad (5-2)$$

For flows in thermal equilibrium, the Maxwellian distribution function can be written as

$$g_s = \rho_s \left( \frac{m_s}{2k\pi T_s} \right)^{\frac{3+N_s}{2}} \exp \left\{ -\frac{m_s}{2kT_s} \left[ \sum_j^3 (u_s^j - U_s^j)^2 + \sum_j^{N_s} (\xi_s^j)^2 \right] \right\} \quad (5-3)$$

which is basically the application of (2-12) to each species. For hypersonic flows in thermal non-equilibrium with the two-temperature model used in [1], however, one has to generalize the Maxwellian distribution function to

$$g_s = \rho_s \left( \frac{m_s}{2k\pi T_s} \right)^{\frac{3+N_s^R}{2}} \left( \frac{m_s}{2k\pi T_{v,s}} \right)^{\frac{N_s^V+N_s^E}{2}} \exp \left\{ -\frac{m_s}{2kT_s} \left[ \sum_j^3 (u_s^j - U_s^j)^2 + \sum_j^{N_s^R} (\xi_s^j)^2 \right] \right. \\ \left. - \frac{m_s}{2kT_{v,s}} \left[ \sum_j^{N_s^V} (\eta_s^j)^2 + \sum_j^{N_s^E} (\zeta_s^j)^2 \right] \right\} \quad (5-4)$$

where  $\xi_s^j$ ,  $\eta_s^j$ ,  $\zeta_s^j$  are rotational, vibrational, and electronic degrees of freedom respectively, and  $N_s^R$ ,  $N_s^V$ ,  $N_s^E$  are the numbers of rotational, vibrational, and electronic degrees of freedom respectively. For electrons,  $T_s = T_{v,s}$ .

The relation between the macroscopic variables like the mass  $\rho_s$ , the momentum  $\rho U^i$ , the total energy  $\rho \epsilon$ , the vibrational-electronic energy  $\rho \epsilon_v$  and the gas distribution function  $f_s$  is

$$Q = \begin{pmatrix} \rho_s \\ \rho U^i \\ \rho \epsilon \\ \rho \epsilon_v \end{pmatrix} = \sum_{s=1}^{11} \int \psi_s f_s d\Xi_s \quad (5-5)$$

where the moments of  $\psi_s$  are given as follows

$$\begin{aligned} \psi_1 &= (1, 0, 0, 0, 0, 0, 0, 0, 0, 0, u_s^i, \sum_{j=1}^3 \frac{(u_s^j)^2}{2} + \sum_{j=1}^{N_s^R} \frac{(\xi_s^j)^2}{2} + \sum_{j=1}^{N_s^V} \frac{(\eta_s^j)^2}{2} + \sum_{j=1}^{N_s^E} \frac{(\zeta_s^j)^2}{2}, \sum_{j=1}^{N_s^V} \frac{(\eta_s^j)^2}{2} + \sum_{j=1}^{N_s^E} \frac{(\zeta_s^j)^2}{2})^T \\ \psi_2 &= (0, 1, 0, 0, 0, 0, 0, 0, 0, 0, u_s^i, \sum_{j=1}^3 \frac{(u_s^j)^2}{2} + \sum_{j=1}^{N_s^R} \frac{(\xi_s^j)^2}{2} + \sum_{j=1}^{N_s^V} \frac{(\eta_s^j)^2}{2} + \sum_{j=1}^{N_s^E} \frac{(\zeta_s^j)^2}{2}, \sum_{j=1}^{N_s^V} \frac{(\eta_s^j)^2}{2} + \sum_{j=1}^{N_s^E} \frac{(\zeta_s^j)^2}{2})^T \\ &\vdots \end{aligned} \quad (5-6)$$

Due to the momentum and energy exchange during particle collisions between all species, however, the Maxwellian distribution functions in (5-4) are not completely independent. Consistent with the physical model used for (5-1), we assume  $g_s$  to have the common velocity and temperatures

$$g_s = \rho_s \left( \frac{m_s}{2k\pi T} \right)^{\frac{3+N_s^R}{2}} \left( \frac{m_s}{2k\pi T_v} \right)^{\frac{N_s^V+N_s^E}{2}} \exp \left\{ -\frac{m_s}{2kT} \left[ \sum_j^3 (u_s^j - U^j)^2 + \sum_j^{N_s^R} (\xi_s^j)^2 \right] - \frac{m_s}{2kT_v} \left[ \sum_j^{N_s^V} (\eta_s^j)^2 + \sum_j^{N_s^E} (\zeta_s^j)^2 \right] \right\} \quad (5-7)$$

Using (5-5), one can find

$$\begin{cases} U^i = \frac{\sum_s^{11} \rho_s U_s^i}{\rho} \\ T = \frac{2 \sum_s^{11} \rho_s (\epsilon_s - \epsilon_{v,s}) - \sum_i^3 \rho (U^i)^2 - 3 \rho_e \frac{k}{m_e} T_v}{\sum_s^{10} (N_s^R + 3) \rho_s k / m_s} \\ T_v = \frac{2 \sum_s^{11} \rho_s \epsilon_{v,s}}{\sum_s^{11} (N_s^V + N_s^E) \rho_s k / m_s} \end{cases} \quad (5-8)$$

The relation between the fluxes of (5-1) and the gas distribution function  $f_s$  is

$$F = \begin{pmatrix} \rho_s U^j - \rho D_s \frac{\partial}{\partial x^j} y_s \\ \rho U^i U^j + p \delta_{ij} - \mu \left( \frac{\partial U^i}{\partial x^j} + \frac{\partial U^j}{\partial x^i} \right) + \frac{2}{3} \mu \frac{\partial U^k}{\partial x^k} \delta_{ij} \\ \rho H U^j - \eta \frac{\partial T}{\partial x^j} - \eta_v \frac{\partial T_v}{\partial x^j} - \rho \sum_{s=1}^{11} h_s D_s \frac{\partial y_s}{\partial x^j} - U^i \mu \left( \frac{\partial U^i}{\partial x^j} + \frac{\partial U^j}{\partial x^i} \right) + \frac{2}{3} U^i \mu \frac{\partial U^k}{\partial x^k} \delta_{ij} \\ \rho \varepsilon_v U^j - \eta_v \frac{\partial T_v}{\partial x^j} - \rho \sum_{s=1}^{11} h_{v,s} D_s \frac{\partial y_s}{\partial x^j} \end{pmatrix} = \sum_{s=1}^{11} \left[ \psi_s u_s^j f_s d\Xi_s \right] \quad (5-9)$$

where  $f_s$  is the Chapman-Enskog expansion up to the Navier-Stokes order like the one given in (2-18).

KFVS scheme can be simply constructed by splitting the flux term of (5-9) into the positive and negative parts according to the sign of the particle velocity

$$F_{j+1/2} = \sum_{s=1}^{11} \left[ \int_{u_s^j > 0} \psi_s u_s^j g_s^L d\Xi_s - \tau \frac{\partial}{\partial t} \left( \int_{u_s^j > 0} \psi_s u_s^j g_s^L d\Xi_s \right) - \tau \frac{\partial}{\partial x^j} \left( \int_{u_s^j > 0} \psi_s (u_s^j)^2 g_s^L d\Xi_s \right) \right. \\ \left. + \int_{u_s^j < 0} \psi_s u_s^j g_s^R d\Xi_s - \tau \frac{\partial}{\partial t} \left( \int_{u_s^j < 0} \psi_s u_s^j g_s^R d\Xi_s \right) - \tau \frac{\partial}{\partial x^j} \left( \int_{u_s^j < 0} \psi_s (u_s^j)^2 g_s^R d\Xi_s \right) \right] \quad (5-10)$$

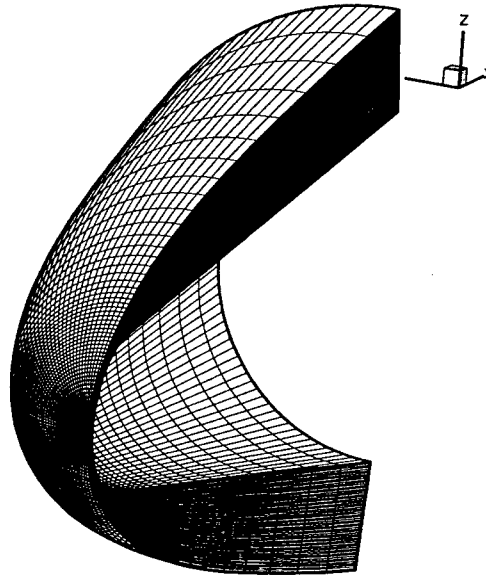
The time derivative term in (5-10) can be replaced by the spatial derivative terms using the following compatibility condition

$$\begin{cases} \frac{\partial \rho_s^{L,R}}{\partial t} = - \frac{\partial}{\partial x^j} [\rho_s^{L,R} (U^j)^{L,R}] \\ \frac{\partial (U^i)^{L,R}}{\partial t} = - (U^j)^{L,R} \frac{\partial (U^i)^{L,R}}{\partial x^j} - \frac{\delta_{ij}}{\rho^{L,R}} \frac{\partial}{\partial x^i} \left( \sum_s^{10} \rho_s^{L,R} \frac{k}{m_s} T^{L,R} + \rho_e^{L,R} \frac{k}{m_e} T_v^{L,R} \right) \\ \frac{\partial T^{L,R}}{\partial t} = - \frac{2}{\sum_s^{10} (N_s^R + 3) \rho_s^{L,R} \frac{k}{m_s}} \left( \sum_s^{10} \rho_s^{L,R} \frac{k}{m_s} T^{L,R} + \rho_e^{L,R} \frac{k}{m_e} T_v^{L,R} \right) \frac{\partial (U^j)^{L,R}}{\partial x^j} - (U^j)^{L,R} \frac{\partial T^{L,R}}{\partial x^j} \\ \frac{\partial T_v^{L,R}}{\partial t} = - (U^j)^{L,R} \frac{\partial T_v^{L,R}}{\partial x^j} \end{cases} \quad (5-11)$$

The thermodynamic relations and chemical kinetic models used in the above KFVS scheme follow the work of Gnoffo et al. in [1-2].

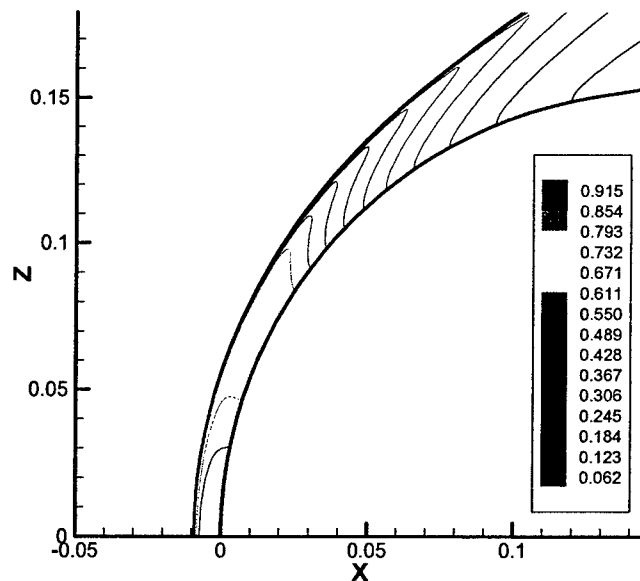
To test this non-equilibrium KFVS scheme, we simulate the RAM-C II flight test case. The configuration is a spherically blunted cone with the nose radius of 0.1524 meter and the half cone angle of 9°. The total length is 1.3 meter. The freestream speed is 7650 m/s. The test case we selected is the one at the altitude of 61 km. As a result, the freestream Mach number is 23.9 and the freestream Reynolds number based on the nose radius is about  $1.95 \times 10^4$ .

Figure 5-1 presents the computational grid used for the computation, which covers half the body for less computational costs. There are 51 points along the streamwise direction, 61 points along the azimuth direction, and 61 points along the normal direction with the first grid spacing of 0.00026 nose radii.



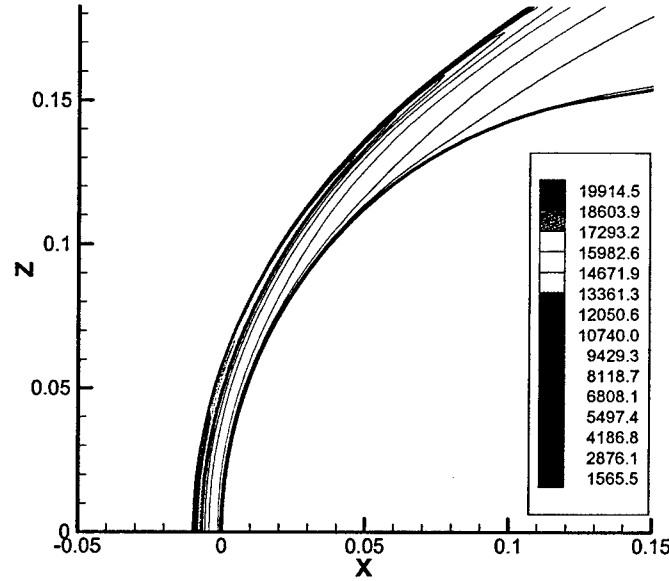
**Figure 5-1 Computational grid**

Figure 5-2 presents the predicted nondimensionalized pressure ( $p / \rho_{\infty} V_{\infty}^2$ ) contours in the first azimuth plane with the fixed wall temperature of 1500°K. The chemical kinetic models used are from [19-20].

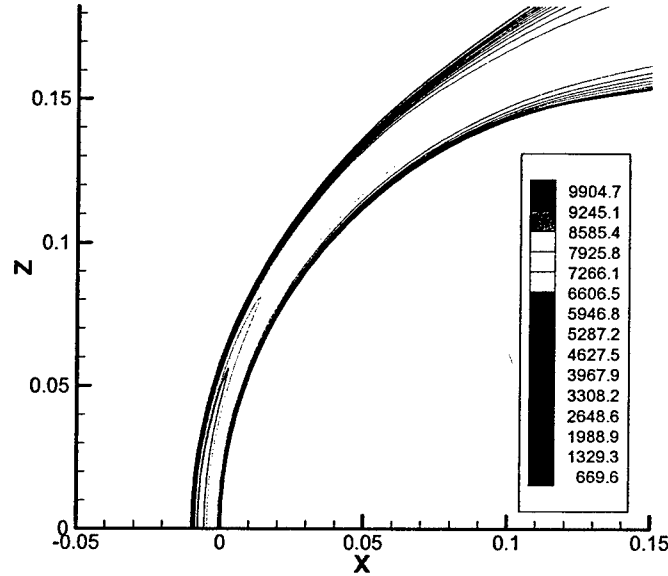


**Figure 5-2 Nondimensionalized pressure ( $p / \rho_{\infty} V_{\infty}^2$ ) contours**

The predicted translational-rotational and vibrational-electronic temperatures are presented in Figure 5-3. The results are consistent with the results obtained in [21-22]. The highest translational-rotational temperature after the shock around the nose can be around 20,000°K whereas the highest vibrational-electronic temperature can be around 10,000°K. In such a high temperature environment, the flow can be weakly ionized.



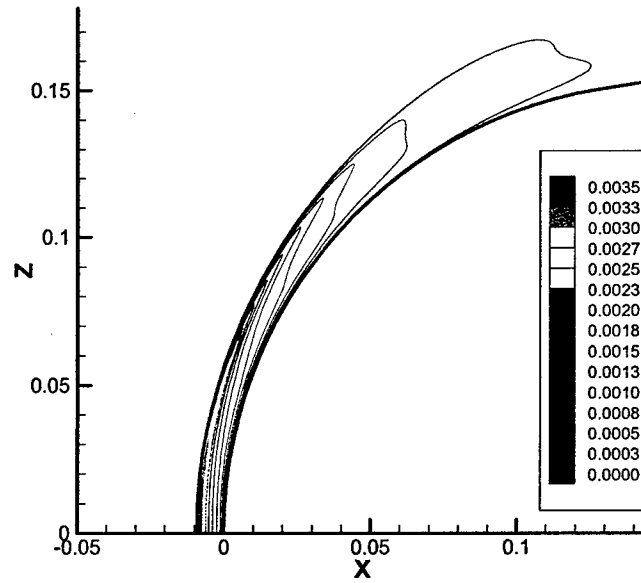
(a) translational-rotational temperature



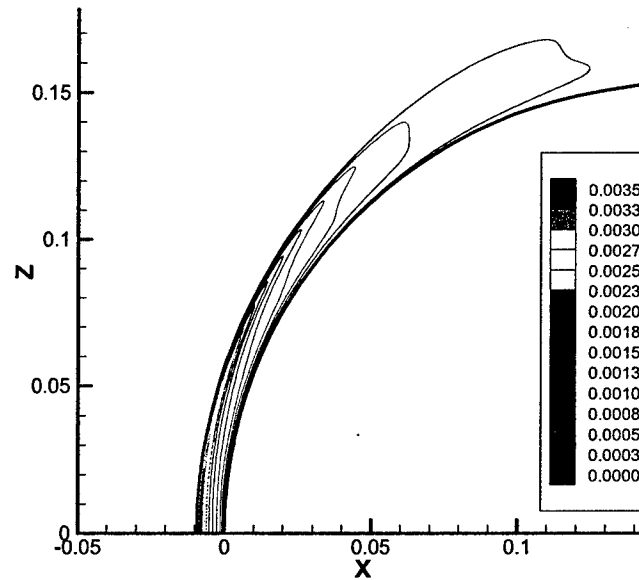
(b) vibrational-electronic temperature

**Figure 5-3 Translational-rotational and vibrational-electronic temperatures**

Figure 5-4 further presents the total ion mass fraction ( $\sum_{s=6}^{10}(\rho_s/m_s)/\sum_{s=1}^{11}(\rho_s/m_s)$ ) contours and the free electron mass fraction ( $(\rho_e/m_e)/\sum_{s=1}^{11}(\rho_s/m_s)$ ) contours. It is found that under the above high temperatures, the ionized particles account for only about 0.7% of the total particles. Such a weak ionization is apparently not enough for electromagnetic flow control. More importantly, Figure 5-4 indicates that the total ion mass fraction is almost the same as the free electron mass fraction. Therefore, the first term of the Lorentz forces added to the momentum equations by Appleton and Bray in [23],  $(n_{ions} - n_e)e(E^i + B^k U^j - B^j U^k)$ , is almost zero. Here  $n_{ions}$  is the total number density of the ions,  $n_e$  is the number density of free electrons, and  $e$  is the electron charge. The electromagnetic effects can be exhibited only through the conduction current density:  $n_e e(U^i - U_e^i)$ .



(a) total ion mass fraction



(b) electron mass fraction

**Figure 5-4 Ions and electron mass fractions**

In the current literatures, the conduction current density is often calculated by the Ohm's law:  $j^i = \sigma(E^i + B^k U^j - B^j U^k)$ . According to the definition of  $\sigma$  in [24], we have computed the electric conductivity for the above RAM-C II case and presented the predicted contours in Figure 5-5. The results are comparable with those given in [24].

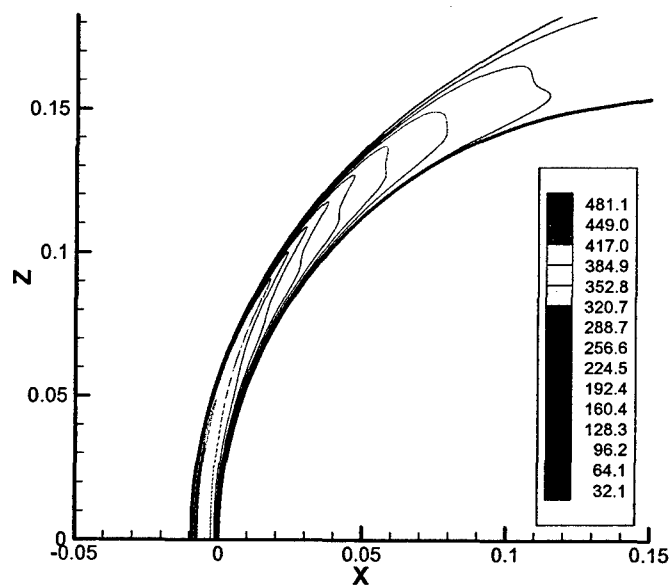


**Figure 5-5 Electrical conductivity**

## 6.0 FUTURE WORK FOR PHASE II

As indicated in Figure 6-1, which is taken from [25], the cylinder and sphere can be considered as simple models of both the wing leading edge and the nose of space vehicles respectively. Therefore, in Phase II, we will first extend the BGK-Burnett scheme to the curvilinear coordinates and use the simpler cylinder case to examine the validity Knudsen number range of the BGK-Burnett scheme. The test data in [26] will be used to validate the BGK-Burnett scheme.

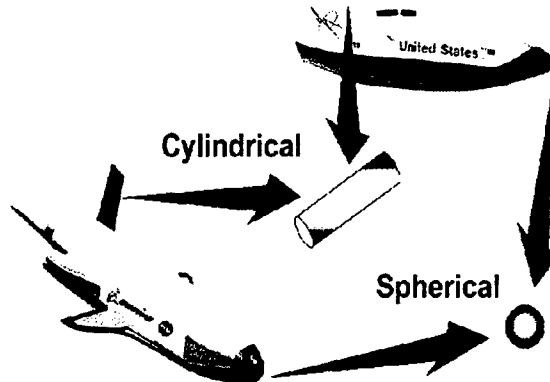


**Figure 6-1 Similarity between simple geometries and wing leading edge/nose of space vehicles [25]**

After the validation, we will extend the BGK-Burnett scheme to magnetogasdynamics in thermal and chemical non-equilibrium and develop an adjoint optimization method based on this solver using a similar approach to the one outlined earlier in this document and ensuring exact discrete consistency between the flow and adjoint solvers on arbitrarily shaped geometries and flow conditions.

## REFERENCES

1. Gnoffo, P.A., Gupta, R.N., and Shinn, J.L., "Conservation Equations and Physical Models for Hypersonic Air Flows in Thermal and Chemical Nonequilibrium," NASA TP-2867, 1989.
2. Cheatwood, F.M., and Gnoffo, P.A., "User's Manual for the Langley Aerothermodynamic Upwind Relaxation Algorithm (LAURA)," NASA TM 4674, 1996.
3. Gaitonde, D.V., and Poggie, J., "Simulation of MHD Flow Control Techniques," AIAA-2000-2326.
4. Poggie, J., and Gaitonde, D.V., "Magnetic Control of Flow Past a Blunt Body: Numerical Validation and Exploration," *Phys. Fluids*, Vol.14 (2002), pp.1720.
5. MacCormack, R.W., "Aerodynamic Flow Calculations with Strong Magnetic Induction and Diffusion," AIAA-2005-0559.
6. Croisille, J-P, Khanfir, R., and Chanteur, G., "Numerical Simulation of the MHD Equations by a Kinetic-type Method," *J. Sci. Comput.*, Vol.10 (1995), pp.81.
7. Xu, K., "A Gas-Kinetic BGK Scheme for the Navier-Stokes Equations and Its Connection with Artificial Dissipation and Godunov Method," *J. Comput. Phys.*, Vol. 171 (2001), pp.289.
8. Vincenti, W.G., and Kruger, C.H., "Introduction to Physical Gas Dynamics," Krieger, Malabar, FL, 1965.
9. Moss, J.N., "Rarefied Hypersonic Flows: Simulations, Experiments, and Applications," *Rarefied Gas Dynamics*, Vol. II, pp. 1123, Oxford University Press, Oxford, 1995.
10. Staack, D., McDaniel, J.C., Glass, C.E., and Miller, C., "Experimental Study of Interacting Rarefied and Continuum Flows," AIAA-2001-2762.
11. Santos, A., Brey, J.J., Kim, C.S., and Dufty, J.W., "Velocity Distribution for a Gas with Steady Heat Flow," *Phys. Rev. A*, Vol.39 (1989), pp.320.
12. Malek, M.M., Baras, F., and Garcia, A.L., "On the Validity of Hydrodynamics in Plane Poiseuille Flows," *Physica A*, Vol.240 (1997), pp.255.
13. Uribe, F.J., and Garcia, A.L., "Burnett Description for Plane Poiseuille Flow," *Phys. Rev. E*, Vol.60 (1999), pp.4063.
14. Aoki, K., Takata, S., and Nakanishi, T., "Poiseuille-type Flow of a Rarefied Gas between Two Parallel Plates Driven by a Uniform External Force," *Phys. Rev. E*, Vol.65 (2002).
15. Zheng, Y., Garcia, A.L., and Alder, B.J., "Comparison of Kinetic Theory and Hydrodynamics for Poiseuille Flow," *J. Stat. Phys.*, Vol.109 (2002), pp.495.
16. Zheng, Y., Garcia, A.L., and Alder, B.J., "Comparison of Kinetic Theory and Hydrodynamics for Poiseuille Flow," *Rarefied Gas Dynamics*, Vol.23 (2002), Whistler, Canada.
17. Ohwada, T., Sone, Y., and Aoki, K., "Numerical Analysis of the Poiseuille Flow and Thermal Transpiration Flows between Two Parallel Plates on the Basis of the Linearized Boltzmann Equation for Hard-sphere Molecules," *Phys. Fluids*, Vol.1 (1989), pp.2042.
18. Zohar, Y., Lee, S.Y.K., Lee, W.Y., Jiang, L., and Tong, P., "Subsonic Gas Flow in a Straight and Uniform Microchannel," *J. Fluid Mech.*, Vol.472 (2002), pp.125.
19. Park, C., "Review of Chemical-Kinetic Problems of Future NASA Missions. I-Earth Entries", *J. Thermo. Heat Trans.*, Vol.7 (1993), pp.385.
20. Gupta, R.N., Yos, J.M., Thompson, R.A., and Lee, K.-P., "A Review of Reaction Rates and Thermodynamic and Transport Properties for an 11-species Air Model for Chemical and Thermal Nonequilibrium Calculations to 30,000K", NASA RP-1232, 1990.
21. Candler, G.V., and MacCormack, R.W., "Computation of Weakly Ionized Hypersonic Flows in Thermochemical Nonequilibrium", *J. Thermo. Heat Trans.*, Vol.5 (1991), pp.266.
22. Josyula, E., and Bailey, W.F., "Governing Equations for Weakly Ionized Plasma Flowfields of Aerospace Vehicles," *J. Spacecraft Rockets*, Vol.40 (2003), pp.845.
23. Appleton, J.P., and Bray, K.N.C., "The Conservation Equations for a Non-equilibrium Plasma", *J. Fluid Mech.*, Vol.20 (1964), pp.659.

24. Macheret, S.O., Shneider, M.N., and Candler, G.V., "Modeling of MHD Power Generation on Board Reentry Vehicles", AIAA-2004-1024.
25. Glass, C.E., and Moss, J.N., "Aerothermodynamic Characteristics in the Hypersonic Continuum-Rarefied Transitional Regime," AIAA-2001-2962.
26. Maslach, G.J., and Schaaf, S.A., "Cylinder Drag in the Transition from Continuum to Free Molecule Flow," *Phys. Fluids*, Vol. 6 (1963), pp.315.
27. Giles, M. B. and Pierce, N. A., "An Introduction to the Adjoint Approach to Design," *Flow, Turbulence and Combustion*, 65:393-415, 2000.
28. Reuther, J. J., Alonso, J. J., Jameson, A., Rimlinger, M. J. and Saunders, D., "Constrained Multi-Point Aerodynamic Shape Optimization using an Adjoint Formulation and Parallel Computers: Part I," *Journal of Aircraft*, 36(1): 51-60, 1999.
29. Kim, S. K., Alonso, J.J., Jameson, A., Design Optimization of High-Lift Configurations Using a Viscous Continuous Adjoint Method, 40th AIAA Aerospace Sciences Meeting & Exhibit, AIAA Paper 2002-0844, Reno, NV, January 2002.
30. Reuther, J. J., Alonso, J. J., Jameson, A., Rimlinger, M. J. and Saunders, D., "Constrained Multi-Point Aerodynamic Shape Optimization using an Adjoint Formulation and Parallel Computers: Part II," *Journal of Aircraft*, 36(1): 61-74, 1999.